A Multiscale Approach for Modeling Scale-Dependent Yield Stress in Polycrystalline Metals

Tetsuya Ohashi[1], Masato Kawamukai[1] and Hussein Zbib[2]

[1)] Kitami Institute of Technology,

Koencho 165, Kitami, Hokkaido, 090-8507 Japan.

ohashi@newton.mech.kitami-it.ac.jp

[2)] School of Mechanical and Materials Engineering,

Washington State University Pullman, WA 99164-2920 USA

zbib@wsu.edu

Abstract

Modeling of scale-dependent characteristics of mechanical properties of metal polycrystals is studied using both discrete dislocation dynamics and continuum crystal plasticity. The initial movements of dislocation arc emitted from a Frank-Read type dislocation source and bounded by surrounding grain boundaries are examined by dislocation dynamics analyses system and we find the minimum resolved shear stress for the FR source to emit at least one closed loop. When the grain size is large enough compared to the size of FR source, the minimum resolved shear stress levels off to a certain value, but when the grain size is close to the size of the FR source, the minimum resolved shear stress shows a sharp increase. These results are modeled into the expression of the critical resolved shear stress of slip systems and continuum mechanics based crystal plasticity analyses of six-grained polycrystal models are made. Results of the crystal plasticity analyses show a distinct increase of macro- and microscopic yield stress for specimens with smaller mean grain diameter. Scale-dependent characteristics of the yield stress and its relation to some control parameters are discussed.

Keywords: A: dislocations, B: crystal plasticity, B: polycrystalline material, B: constitutive behaviour, B: scale dependency

1. Introduction

Scale-dependent characteristics of mechanical properties of metal polycrystals are well known and are summarized in the form of a Hall-Petch type relation,

$$\sigma = \sigma_0 + k\bar{d}^{-1/2}, \qquad (1)$$

where σ denotes strength-related physical quantity such as yield stress, plastic flow stress, tensile strength, and $\bar{d}$ denotes the average grain diameter of the polycrystal or another length scale. In recent years, there have been many efforts to model such effects into the theory of continuum mechanics, and among them, introduction of the concept of plastic strain gradient, or more directly the concept of geometrically necessary dislocations (GNDs), into the framework of the theory induced a wide range of discussion. Density of GNDs has been incorporated in the expression of flow stress (Fleck et al. 1994; Gao et al. 1999; Shu and Fleck, 1999), strain hardening (Acharya and Beaudoin, 2000; Acharya, Bassani and Beaudoin, 2003; Ohashi, 2004a; Ohashi, 2005; Akasheh, Zbib and Ohashi, 2006), or free energy (Shizawa and Zbib, 1999; Gurtin, 2002; Mesarovic, 2005). Among them, Ohashi (2004a) introduced a new model of crystal plasticity analysis where not only the statistically stored dislocations (SSDs) but also GNDs contributed to the mean free path of moving dislocations, and we successfully reproduced the Hall-Petch type relation of plastic flow stress level. However, scale-dependent characteristics of yield stresses are not yet fully understood in terms of mechanics and there are a lot of points to be studied (for example, Fredriksson and Gudmundson, 2005; Cheong, *et al*., 2005; Khan, *et al*., 2006; Berbenni *et al*., 2006).

Let us consider the first step of slip deformation in a crystal grain. There should be a variety of defects, including pinned dislocations. Among them, a certain dislocation segment may act as a multiplication source of dislocations when the resolved shear stress on it reaches a critical value. When the grain size is infinite and the lattice friction stress for dislocation movement is zero, a

Frank-Read type dislocation source (abbreviated hereafter as FR source) with size λ starts to emit dislocation loops when the resolved shear stress reaches the value (for example, Hull and Bacon, 2001)

$$\tau_{\infty} = \frac{\mu \tilde{b}}{\lambda}, \qquad (2)$$

where μ and $\tilde{b}$ denote the elastic shear modulus and the magnitude of Burgers vector, respectively. The larger the source size λ is the smaller is the critical resolved shear stress. If the size of the crystal grain is finite, the dislocation source length cannot be larger than the grain size, and this fact brings about a strong size effect of yield stress and strain hardening in single crystals (Uchic *et al*., 2004; Benzerga, 2005). Similar and even more complex phenomena are thought to take place in crystal grains in polycrystals (Ohashi and Kawamukai, 2005). As dislocations are emitted from a dislocation source situated inside a grain, they will propagate outwards from the source until they hit grain boundaries which cause resistance to the further movement of dislocations and subsequent emission from the source.

In this paper, we first focus on the initial movement of a dislocation arc that expands from a FR source and its interaction with grain boundaries. To simulate such a process, we use a dislocation dynamics software code and find the minimum resolved shear stress for the FR source to emit at least one closed loop. Results of the dislocation dynamics simulations are then modeled into the expression of critical resolved shear stress of slip systems, which is used in the continuum mechanics-based crystal plasticity analyses of a six-grained polycrystal model under tensile load. Scale-dependent characteristics of yield stress and their relation to some influencing parameters are discussed.

2. Discrete Dislocation dynamics

2.1 A cuboidal-shaped crystal grain with a Frank-Read type dislocation source

Let us assume a cuboidal-shaped single crystal specimen of copper (Fig. 1(a)). Material constants are listed in Table 1. Crystal orientation is chosen so that the xy-cross section is parallel to the slip plane (111) and the y axis is parallel to the slip direction $[\bar{1}10]$. Six surfaces of the specimen are assumed to correspond to grain boundaries, and movement of dislocations is confined to the interior of the specimen. Image force arising from grain boundaries is neglected in this simulation because it is small compared to the forces generated by bending of the dislocation line or back stress from piled up dislocations. The dimension of the slip plane which is trimmed by four grain boundary planes is $d \times d$ and a dislocation segment of length λ is placed on it. Dislocation lines cannot end within the grain interior, but the segment should be connected to other segments (Fig. 1(a)). However, in this simulation, only the segment aa', which is shown by a solid line in Fig. 1(a), is considered for simplicity. Both ends of the dislocation segment aa' are assumed to be pinned and cannot move. In this condition, the dislocation segment aa' acts as a Frank-Read type dislocation source, and we simulate the movement of dislocations when a constant shear stress $\tau = \tau_{yz}$ is applied to the specimen. The dislocation dynamics simulation package MDDP (Zbib and de la Rubia 2002, Zbib and Khraishi, 2005) is used.

By the dislocation dynamics technique, we solve the movement and interaction of dislocation lines during a small interval of time with piecewise linear approximation and repeat the process. A dislocation line is divided into small segments and the main governing equation for the dynamics of each segment is given by (Hirth, Zbib and Lothe, 1998; Zbib and Khraishi, 2005),

$$m_s \dot{\mathbf{v}}_s + \frac{1}{M_s(T,p)} \mathbf{v}_s = \left[\left(\sum_{\substack{n=1 \\ n \neq s}}^{N_s} \overset{d\,(n)}{\sigma} \right) + \overset{a\,(s)}{\sigma} \right] \cdot \mathbf{b}_s \times \boldsymbol{\xi}_s . \quad (3)$$

Here, $\mathbf{v}_s$ is dislocation segment velocity, m_s is effective mass of the dislocation segment which depend on the dislocation character (Hirth, Zbib and Lothe, 1998), M_s is mobility, $\overset{a\,(s)}{\sigma}$ is the

stress by applied force, $\overset{d\,(n)}{\sigma}$ is the stress generated by dislocation segment n (Hirth and Lothe, 1982), and $\mathbf{b}_s$ and $\boldsymbol{\xi}_s$ denote unit vectors parallel to the slip direction and the dislocation segment.

2.2 Confinement of dislocation movement by grain boundaries

Among possible sites for the FR sources, we first place the source at the center of the specimen and simulate the emission of dislocation loop(s). Fig. 2(a)-(c) show snap shots for the case when $\lambda = 0.2\mu m$, $d = 1\mu m$ and $\tau = 1.027\tau_\infty$. Some parts of the dislocation line hit grain boundary planes (Fig. 2(b)), but the dislocation continues to expand and makes up a closed loop (Fig. 2(c)). Fig. 3 shows the results when $\lambda = 0.5\mu m$, $d = 1\mu m$, and $\tau = 1.9\tau_\infty$. In contrast to the results shown in Fig. 2, growth of the dislocation arc stopped after it hit grain boundaries and makes the shape shown in Fig. 3. When we increase the applied stress to $\tau = 2.32\tau_\infty$ the dislocation expands and forms a closed loop.

Fig. 4(a) and (b) show growths of dislocation arcs from two FR sources at different positions. Grain size, FR source length and applied stress in these two cases are the same ($\lambda = 0.2\mu m$, $d = 1\mu m$, $\tau = 1.027\tau_\infty$). In the case shown in Fig. 4(a), the dislocation arc stopped growing at the initial stage, while the dislocation arc grown from the FR source shown in Fig. 4(b) swept about 93% of the area of the slip plane. This comparison shows that the area fraction swept by a dislocation arc depends not only on the size ratio of the FR source length to grain diameter but also on the position where the FR source is placed. The applied stress required to form a closed dislocation loop from a FR source is reduced when the FR source is positioned at the center of the grain.

Fig. 5 shows the results when two FR sources belonging to the same slip system and with the same size, $\lambda = 0.2\mu m$, are placed in a sufficiently large crystal grain with $d = 25\mu m$. $\tau = 1.16\tau_\infty$ is applied. The distance between the slip planes where two FR sources lie is $0.25\mu m$, and the distance between the FR sources in the slip direction is $2.5\mu m$. The two FR sources emit dislocation loops but notable interaction is not observed.

Let us assume a crystal grain with a certain grain size and assume that there can be FR sources with any size smaller than the grain. We also assume that FR sources can take any position inside the grain and applied stress gradually increases from zero. On one hand, the FR source with the largest size will become activated before the smaller ones, because τ_∞ is inversely proportional to the size λ of the FR source. On the other hand, a *large* FR source with a size as large as the grain diameter cannot fully operate to form a closed loop at an initial stage of yield, since some parts of the dislocation arc may hit the grain boundaries at an early stage of its growth and it cannot fully grow until shear stress much larger than τ_∞ is applied and, subsequently, smaller FR sources may be activated. The foregoing discussion indicates that there is an optimal size of FR source between zero and the grain size, from which a fully developed dislocation loop can be formed at the minimum stress level. Such a FR source should be placed somewhere near the center of the grain.

We simulate dislocation emission from a FR source that is placed at the center of the grain. Various combinations of sizes for FR source and grain are chosen. A certain shear stress is applied and kept constant throughout the simulation while the FR source emits dislocation arc. The maximum number of steps of dislocation dynamics simulation used in this study is 750,000 for most cases and 3,000,000 and 7,500,000 for a few cases. When the applied stress is less than a certain critical value, the dislocation arc emitted from the FR source stops growing before it makes a complete loop. While when the applied stress is larger than the critical value, the FR source may emit more than one closed loop. There is a minimum shear stress (critical stress) at which the FR source emits only one closed loop. Such stress level τ_{thresh} for various conditions of grain and FR source sizes are searched by DD simulation combined with the following idea of bisection algorithm (Press, *et. al,* 1996).

1. We apply a relatively large constant shear stress τ_R to the model, and observe a dislocation loop is emitted.
2. We then apply a relatively small stress τ_L and confirm that dislocation loop is *not* emitted during the maximum DD step.

3. Then, we apply $\tau_M = (\tau_R + \tau_L)/2$ and observe if a loop is emitted within the maximum DD step.

4. If a loop is emitted at τ_M, we rename τ_M as τ_R. If a loop is not emitted, we rename τ_M as τ_L.

5. Loop back to the step 3 until $|\tau_R - \tau_L|$ is small enough.

After a several times of loop-back, we obtain a threshold (lowest) stress at which FR source emit a dislocation loop within a limited number of DD steps.

The results obtained are shown in Fig. 6, where data obtained with the simulation limit of 750,000 steps are plotted by solid symbols, while the one obtained with the limit of 7,500,000 steps is plotted by an open symbol. DD simulations data for the time needed to emit a dislocation loop from a FR source with various lengths and placed in a grain of size *d* are summarized in Table 2.

In the case where FR source length $\lambda = 0.3\mu m$, $\tau_{thresh}/\tau_\infty$ levels off to approximately unity when the ratio of grain size to FR source length is sufficiently large ($d/\lambda \gg 3$). A dislocation loop is quickly generated after the application of shear stress; for example, when $d/\lambda = 6$, the FR source emits a closed loop at stress level $\tau_{thresh}/\tau_\infty \approx 1.07$ and the time needed to form the loop t_{emit} is about 0.5×10^{-6} seconds. When an FR source of the same size ($\lambda = 0.3\mu m$) is placed in a smaller grain, larger shear stress is needed for the formation of a closed dislocation loop. When $d/\lambda = 3$, $\tau_{thresh}/\tau_\infty$ is about 1.3.

In the case where FR source length λ is equal to $0.5\mu m$, $\tau_{thresh}/\tau_\infty$ levels off to about 1.2 when grain size is large enough ($d/\lambda \gg 3$). When the grain size is smaller and the ratio to the FR source length d/λ approaches 3, $\tau_{thresh}/\tau_\infty$ starts to increase and $\tau_{thresh}/\tau_\infty$ is approximately 2.3 when $d/\lambda = 2$.

When $\lambda = 10\mu m$, it takes a much longer time for a FR source to emit a dislocation loop compared to the case when $\lambda = 0.3$ or $0.5\mu m$. In the case where $d/\lambda = 10$ with 750,000

steps as the limit of the simulation, $\tau_{thresh}/\tau_{\infty} \approx 2$ (to be discussed below) and the time needed to generate a dislocation loop after the application of shear stress is 2.5×10^{-4} seconds, which is about 500-times longer than that in the case where $\lambda = 0.3\mu m$ and $d/\lambda = 6$. If we increase the limit of simulation steps to 7,500,000, the level-off stress decreases to $\tau_{thresh}/\tau_{\infty} \approx 1.5$, which is indicated by the symbol $\triangle$ in Fig. 6, and the time needed to generate a dislocation loop after the application of shear stress is 3.7×10^{-3} seconds. These differences in level-off stress and time needed to emit a dislocation loop suggest that the movement of dislocation has a viscous character, which we will discuss later. When the FR source length is kept constant ($\lambda = 10\mu m$) and the grain size is decreased, the ratio $\tau_{thresh}/\tau_{\infty}$ starts to increase at $d/\lambda \approx 3$, which is the same as the cases for $\lambda = 0.3$ or $0.5\mu m$. When $d/\lambda = 2$, the ratio $\tau_{thresh}/\tau_{\infty}$ is about 3.5.

The above results are summarized as follows. When the ratio of the grain size to FR source length is sufficiently large ($d/\lambda \gg 3$), the stress needed for a FR source to emit a dislocation loop does not depend on the grain size, while in the region $d/\lambda < 3$, $\tau_{thresh}/\tau_{\infty}$ rapidly increases with reduction of grain size. This result indicates that a FR source with source length λ larger than 3rd of the grain diameter d requires a much larger shear stress than that given in eq. (2) to emit a dislocation loop. This fact, in turn, indicates that when shear stress is gradually applied to a crystal grain with a certain grain diameter, a FR source with length nearly equal to 3rd of the grain diameter and positioned near the center of the grain emits the first dislocation loop. The time needed to emit a dislocation loop varies significantly with the source length, grain size and the applied stress, however a quantitative understanding of this is not yet enough[1].

The mechanism for the sharp increase in $\tau_{thresh}/\tau_{\infty}$ at $d/\lambda \approx 3$ is thought to be as follows. The distance h between the end point of the FR source and the grain boundary is equal to

[1] We note that some of the data for $d/\lambda \gg 3$ give results for t_{emit} that follow the linear model proposed by Benzerga, et al., 2004 which assumes that the shape of the dislocation loop is ellipse. But, in general, the DD result we obtained is for the formation of complete loops whose geometries is far from being approximated as ellipse when the dislocation interacts with the boundary as shown in Fig.

$h = (d - \lambda)/2$. When τ_∞ is applied, the loop will wrap around until it hits the wall as shown in Fig. 3. If $h > \lambda$ then the loop will continue to go through the gap h. On the other hand, if $h < \lambda$, the loop will stop and in order to propagate the loop further the stress must be increased. The increase in stress for the emission of the first loop through the "gap" is a result of insufficient space for dislocation movement. In other words, the increase is caused by the fact that the dislocation line must bend sharply in a tight area of size *h* and it requires a higher stress level. If $h > \lambda$ is the condition for (more or less) free expansion of the dislocation arc, then the threshold for the sharp increase in $\tau_{thresh}/\tau_\infty$ occurs when $d/\lambda \geq 3$. In fact, Fig. 4 actually shows a sharp increase at $d/\lambda = 3$. Therefore, the value of *h* relative to λ primarily controls the process. When the first loop is formed, it would be even harder for a second loop to propagate since the first loop would be exerting a back stress at the FR source.

2.3 Level-off stress when the grain size is sufficiently large compared to the size of the Frank-Read source

The stress needed for the FR source to emit a dislocation loop levels off to a certain value when $d/\lambda \gg 3$, as already shown in Fig. 6, and depends on the size of the FR source. The reason for this dependency on FR-source size is as follows. For example, for $\lambda = 0.3\mu m$ and $10\mu m$ the corresponding values of τ_∞ are 40.25 and 1.21 MPa, respectively. This stress arises from the line tension of bent dislocations. At the same time, dislocations have to overcome the lattice friction stress when they move. The lattice friction stress for face centered cubic crystals is approximately equal to $10^{-5}\mu$, where μ denotes elastic shear modulus, and the value for the material considered in this study is about 0.483 MPa (Table 1). When $\lambda = 0.3\mu m$, this friction stress is negligibly small compared to τ_∞ (=40.25 MPa), while in the case where $\lambda = 10\mu m$, the friction stress is about $0.4\tau_\infty$. Therefore, the threshold stress τ_{thresh} to emit a dislocation loop needed for an FR

2(b).

source with $\lambda = 10\mu m$ is roughly estimated as $1.4\tau_\infty$.

The value for the ratio $\tau_{thresh}/\tau_\infty$ obtained by the dislocation dynamics simulation for the case where $\lambda = 10\mu m$ is about 1.5 when the limit of simulation steps is 7,500,000 and larger shear stress is needed to emit a dislocation loop in a shorter duration. That is, the effect of lattice friction stress on emission of a dislocation loop plays an important role when the FR source length is large and the movements of dislocations become viscous. When the stress

$$\tau_\infty + \text{(lattice friction stress)} \qquad (4)$$

is applied to the FR source, it will emit a dislocation loop after a long period of time, but more stress than that given in eq. (4) is needed to emit a dislocation loop in a finite period of time. Therefore, the level-off stress for the $d/\lambda \gg 3$ region depends not only on the FR source length and lattice friction stress but also on strain rate.

Let us denote the level-off stress when $d/\lambda \gg 3$ as τ_{loff} and define the ratio of τ_{loff} and τ_∞ as β:

$$\tau_{loff} = \beta\tau_\infty = \beta\frac{\mu\tilde{b}}{\lambda}. \qquad (5)$$

β is a non-dimensional number and, in general, depends not only on the lattice friction stress (material parameter) and strain rate but also on the character of the FR source (edge, screw, or mixed-type dislocation segment), and the shape of the dislocation arc emitted from the source, because the elastic strain energy that accompanies the dislocation arc depends on these factors. The fact that β depends on the lattice friction stress results in its dependency on sizes of the FR source and crystal grain. Fig. 7 shows $\log(\beta)$, β being obtained by the dislocation dynamics simulation, plotted against $\log(\lambda)$. The gradient of this plot is, however, small and ranges

between 0.1 and 0.3.

3. Scale dependent yield stress of polycrystals

3.1 Implementation of the dislocation dynamics results into a crystal plasticity model

In the previous section, dislocation multiplication inside a grain was simulated and the relations between grain size, dislocation source length and critical resolved shear stress were examined. In this section, we apply the results obtained in the previous section to analyze scale-dependent properties of yield phenomena of polycrystals by continuum mechanics-based crystal plasticity analyses.

In crystal plasticity analyses, the critical resolved shear stress for slip system *n* has been given by the modified Bailey-Hirsch model (Ohashi, 1994):

$$\theta^{(n)} = \theta_0(T) + \sum_{m=1}^{12} \Omega^{(nm)} a\mu\tilde{b}\sqrt{\rho_S^{(m)}}\,, \tag{6}$$

where the first term in the right hand side of eq. (6) stands for lattice friction stress for moving dislocations and the second term defines slip resistance of statistically stored (SS) dislocations on twelve slip systems against moving ones on the slip system *n*. $\rho_S^{(m)}$ denotes the density of SS dislocations accumulated on the slip system *m*, $\mathbf{\Omega}$ gives the interaction matrix between slip systems, and a is a numerical factor of the order of 0.1.

Increment of the SS dislocation density is given by

$$\dot{\rho}_S^{(n)} = c\dot{\gamma}^{(n)} / \tilde{b}L^{(n)}\,, \tag{7}$$

where $\dot{\gamma}^{(n)}$ and c denote increment of shear strain and a numerical constant of order 1, respectively. $L^{(n)}$ is the mean free path of moving dislocations on slip system *n* and is defined by

(Ohashi, 2004a; Ohashi, 2005)

$$L^{(n)} = \frac{c^*}{\sqrt{\sum_j w^{(jn)} \left(\rho_S^{(j)} + \left\| \rho_G^{(j)} \right\| \right)}}, \tag{8}$$

where c^* is a numerical constant of the order of 10-100. $\left\| \rho_G^{(j)} \right\|$ denotes the density norm of the geometrically necessary (GN) dislocations on slip system j and is defined as follows (Ohashi, 1997):

$$\left\| \rho_G^{(n)} \right\| = \sqrt{\left(\rho_{G,edge}^{(n)} \right)^2 + \left(\rho_{G,screw}^{(n)} \right)^2}, \tag{9}$$

where $\rho_{G,edge}^{(n)}$ and $\rho_{G,screw}^{(n)}$ denote the edge and screw components of the GN dislocations on the n-th slip system and are defined by

$$\rho_{G,edge}^{(n)} = -\frac{1}{\tilde{b}} \frac{\partial \gamma^{(n)}}{\partial \xi^{(n)}}, \quad \rho_{G,screw}^{(n)} = \frac{1}{\tilde{b}} \frac{\partial \gamma^{(n)}}{\partial \zeta^{(n)}}. \tag{10}$$

Here, $\xi^{(n)}$ and $\zeta^{(n)}$ denote directions parallel and perpendicular to the slip direction on the slip plane, respectively.

The weight matrix $w^{(jn)}$ controls the contribution of SS and GN dislocations accumulated on the slip system j to the mean free path of moving dislocations on slip system n. Usually, dislocations on self- and coplanar slip systems are not considered to contribute to the mean free path, and this assumption is also used in this paper. Details of dislocation models are given elsewhere (Ohashi, 2004b; 2005). Let us extend the expression given in eq. (6) and include the characteristics of the early stage of dislocation multiplication within a crystal grain.

The shear stress needed for a FR source to emit a dislocation loop is a function of d and λ as already shown in Fig. 6, and it levels off to the value given in eq. (5) when $d/\lambda \gg 3$. Let us simplify this result as follows: when the shear stress given in eq. (5) is applied, FR sources that satisfy $d/\lambda \geq 3$ will emit dislocation loops and other FR sources will not. Further, let us assume that there are FR sources of any possible size in a crystal grain of size d. When shear stress gradually increases, the FR source which satisfies $d/\lambda \geq 3$ and has the maximum size of λ will be the first to emit a dislocation loop. This means that a FR source with size $d/\lambda = 3$ will emit a dislocation loop first[2]. The minimum shear stress needed to emit a dislocation loop is then given by

$$\tau = \beta \frac{\mu \tilde{b}}{(d/3)} = 3\beta \frac{\mu \tilde{b}}{d}, \qquad (11)$$

when there are no obstacles to the expansion of a dislocation arc other than grain boundaries. In cases where there is a high density of grown-in dislocations or other obstacles and slip resistance to dislocation movement due to these is large enough compared to the stress level given by eq. (11), then the stress needed to activate FR sources does not play an important role and the right hand side terms in eq. (6) will approximately define the slip resistance. On the other hand, if the density of obstacles to the movement of dislocations is very small and grain boundaries play a major role in the movement and expansion of dislocation arcs, the stress given by eq. (11) will be a good

[2] Dislocations begin to move under application of a stress smaller than τ_∞, but the contribution of this movement to plastic strain increment is limited because the area swept by dislocation lines is small and dislocations stop their movement at their equilibrium shape under the applied stress. In other words, just a small amount of dislocation movement does not mean the yielding, but avalanche of movement of dislocations is needed to deliver a meaningful amount of plastic strain increment. Transition from the small movement of dislocations to the avalanche of them should not be catastrophic but the formation of closed dislocation loop makes a significant difference because the FR source, from which a dislocation loop was emitted, can emit next dislocation loop and repeat this process at the same stress level, even if the time needed to emit the next loop will be longer because of the back stress from the piled-up one. Application of τ_{thresh} will make the FR source to emit the first dislocation loop and this stress serve as an appropriate measure for the yield stress.

approximation for the critical resolved shear stress. If dislocation movement takes place in such a manner that the dislocation arc has to interact with many grown-in dislocations or other obstacles before it hits grain boundaries or the dislocation arc moves freely inside the grain until it hits the grain boundary, then we can use the following model for the critical resolved shear stress:

$$\theta^{(n)} = \mathrm{Max}\left[\theta_0(T) + \sum_{m=1}^{12}\Omega^{(nm)}a\mu\tilde{b}\sqrt{\rho_S^{(m)}},\ 3\beta\frac{\mu\tilde{b}}{d}\right]. \qquad (12a)$$

On the contrary to the above situation, if slip resistance by grown-in dislocations or other obstacles play as much of a role as the grain boundaries do, we can simply add this slip resistance to give

$$\theta^{(n)} = \theta_0(T) + \sum_{m=1}^{12}\Omega^{(nm)}a\mu\tilde{b}\sqrt{\rho_S^{(m)}} + 3\beta\frac{\mu\tilde{b}}{d}. \qquad (12b)$$

In the following discussion, we use eq. (12b) as an extended expression of the Bailey-Hirsch type model of critical resolved shear stress.

3.2 Polycrystal models employed for the crystal plasticity analysis

Fig. 8 shows the polycrystal model employed in this study. The aspect ratio of the model is W:H:D = 5:15:1, and three different specimens with W=1, 5, or 50 μm are used. The width W is considered to be the mean grain diameter $\bar{d}$ of the specimen. Each crystal grain is a polygonal plate, and their representative size d, which is used in eq. (12b), is calculated by

$$\pi\left(\frac{d}{2}\right)^2 = (area\ of\ polygon). \qquad (13)$$

In the following analyses, we assume for simplicity that $\beta = 1$ and does not depend on grain size. We also analyze slip deformation with $\beta = 0$ for comparison. Data used for the continuum mechanics crystal plasticity analyses are summarized in Table 3. The first term in the right hand side of eq. (12b) is assumed to be 0.483 MPa, which is for the lattice friction stress and is consistent with the value used in the dislocation dynamics simulation. An isotropic hardening condition is used for the interaction matrix $\Omega^{(nm)}$, and $a = 0.3$. Elastic shear modulus μ is given by the inverse of an elastic compliance datum s_{44}. This value of elastic shear modulus is about 1.6-times larger than that used for DD simulation. Three cases for the initial density of dislocations 1×10^{11}, 1×10^{12} or 1×10^{13} m^{-2} are assumed. Dislocations initially are distributed uniformly on each slip system in every grains. The total of initial dislocation densities ρ_0^{total} is 1.2 $\times10^{12}$, 1.2×10^{13} or 1.2×10^{14} m^{-2}, respectively.

Specimens are divided into 4864 finite elements of eight node composite type. The bottom surface (y=0) of the specimen is fixed in the y-direction, while a uniform tensile displacement is given on the top surface (y=H). Slip deformations of the specimens are analyzed until the specimens show macroscopic yield.

3.3 Results and discussion of crystal plasticity analyses

Fig. 9 shows nominal stress vs. nominal strain curves when $\beta = 0$. The initial dislocation density is 1×10^{12} m^{-2} on each slip system and ρ_0^{total} is 1.2×10^{13} m^{-2}. Deformation curves before yielding are the same for the three specimens (Fig. 9(a)), and they begin to show a slightly different strain hardening behavior after the yield point. This difference in strain hardening behavior comes from the contribution of GN dislocations to the mean free path of moving dislocations (eq. (8)). With the development of plastic deformation (Fig. 9(b), Ohashi, 2004a), contribution of GN dislocations to the strain hardening becomes distinct and this contribution is more significant in specimens with smaller mean grain diameter.

Fig. 10 shows nominal stress vs. nominal strain curves obtained when $\beta = 1$ and $\rho_0^{total} = 1.2 \times 10^{12}, m^{-2}$. Macroscopic yield points for the specimens with mean grain diameter $\bar{d}(= W) = 1$, 5 and 50 μm are indicated by A', B' and C', respectively. A, B and C in the same figure indicate the points where the first plastic slip takes place in each specimen. Slip deformation occurs only locally in the specimen during the loading period from A to A', B to B', or C to C', and plastic shear strain (pre-yield micro strain) is small compared to the elastic one. Let us call the points A, B and C microscopic yield points and the points A', B' and C' macroscopic yield points. The smaller the mean grain diameter is the larger are the macroscopic and microscopic yield points.

Fig. 11 (a) and (b) show stress-strain curves when the total initial dislocation densities are 1.2×10^{13} and $1.2 \times 10^{14}\,\mathrm{m}^{-2}$, respectively. Scale-dependent characteristics of the macro- or microscopic yield stresses become less prominent for large initial dislocation density. This effect is due to the fact that the second term in the right hand side of eq. (12b) becomes to play more important roles when the initial dislocation density is larger and the contribution of the third term becomes relatively small. Let us think about a simplified condition that $\theta_0 = 0$, $\Omega^{(nm)} = 1, (n, m = 1,.....,12)$, a=0.3 and β=1. The CRSS before slip deformation is given by, from eq. (12b),

$$\theta_{yield} = 3(1.2\sqrt{\rho_0} + 1/d)\mu\tilde{b},$$

where ρ_0 denotes the initial dislocation density which is uniformly given for each slip system. It is noted that $\sqrt{\rho_0}$ and $1/d$ have the same dimension. If the initial dislocation density is very low and $\sqrt{\rho_0}$ is negligibly small compared to $1/d$ (small grain size and low dislocation density), θ_{yield} will show $1/d$ dependence. If, on the other hand, $\sqrt{\rho_0}$ is much larger than $1/d$ (large grain size and high dislocation density), θ_{yield} will show only a weak scale dependence. In the cases in between the above mentioned two extremes, $\log(\theta_{yield})$ plotted against $\log(d)$ will show non-linear dependence and their gradient change between 0 and 1 depending on d and the initial

dislocation density.

Similar things happen during plastic deformation. With the progress of plastic deformation, dislocation density increase and the effect of grain boundaries will become relatively small. It is interesting to note that eq. (12b) shows the effect of accumulated dislocations to the CRSS becomes comparable to that of grain boundaries when $\sum_m \sqrt{\rho_S^{(m)}} \approx \frac{1}{d}$, as far as the values for $\Omega^{(nm)}$ is close to unity, $a \approx 0.3$ and $\beta \approx 1$. After this point of deformation, effect of the accumulated dislocations predominates in the CRSS.

Fig. 12 summarizes the macro- and microscopic yield stresses as functions of the mean grain diameter and total initial dislocation density. The gradient of the curves shown in Fig. 12 is close to -0.5 and approximately follows the Hall-Petch relation when the total initial dislocation density is less than 10^{13} m^{-2} and the mean grain diameter is within a range between one to a few μm. When the total initial dislocation density is as large as 10^{14} m^{-2} or when the mean grain diameter is larger than 10 μm, the grain size exponent of the yield stress deviates from -0.5 and scale dependency diminishes.

3.4 Effects of grown-in and piled-up dislocations on moving dislocations

In section 2, we obtained the results shown in Fig. 6 by considering a simplified condition where only a single FR source existed in an otherwise perfect crystal grain and each part of dislocation segment interacts only with other parts of the dislocation line and grain boundaries. In real metal crystals, there usually exist grown-in dislocations before the plastic slip starts. Such dislocations interact with the dislocation arc emitted from the FR source and act as a barrier to its movement. This effect will result in an increase in viscosity for the movement of the dislocation arc, and grown-in dislocations will thus cause an increase in the level-off stress. Then, β given in eq. (12b) depends not only on strain rate, lattice friction, dislocation source characteristics and grain diameter, but also on the initial density of dislocations:

$$\beta = \beta(\dot{\gamma}, d, \rho_0, ...) . \qquad (14)$$

It must also be noted that a piled-up dislocation, which has been emitted from an FR source, will build up a back stress not only to the source from which it was emitted but also to sources in neighboring grains and lessen the effective shear stress for the emission of next dislocation loop. As a result of this, a FR source that already emitted a dislocation loop will need longer time, or be difficult, to emit the second loop at the same stress level. Therefore, if the number of FR sources that operate at an early stage of yield is limited to be small, the numerical value in eq. (11) must be larger than 3.

Confinement of the movement of dislocations by grain boundaries will also have significant effects on the plastic slip phenomena after macroscopic yield. For example, the mean free path of dislocations can not exceed the grain diameter and the model given by eq. (8) is revised as

$$L^{(n)} = \mathrm{Min}\left[\frac{c^*}{\sqrt{\sum_j w^{(jn)} \left(\rho_S^{(j)} + \left\| \rho_G^{(j)} \right\| \right)}}, \frac{d}{2} \right] . \qquad (15)$$

While eq. (8) accounts for the scale-dependent characteristics of strain hardening in terms of GN dislocations (Ohashi, 2004a), eq. (15) also captures the grain boundary effect to the dislocation mean free path. This dependency causes another underlying factor for the macroscopic scale-dependent characteristics of metal polycrystals. Further study is needed to clarify these effects.

4. Summary

Mechanisms for the scale-dependent characteristics of yield stress of FCC-type metal

polycrystals were studied, and movement of a dislocation arc emitted from a Frank-Read type dislocation source within a grain was simulated by dislocation dynamics. The results were then used to extend the Bailey-Hirsch type expression for the critical resolved shear stresses for slip deformation, and crystal plasticity analyses of tensile tests of six-grained polycrystal models were performed. Results of the crystal plasticity analyses showed clear scale-dependent characteristics of yield stress. Exponent of the grain size was dependent on the initial dislocation density and also on the mean grain diameter.

Acknowledgements

Dr. Michiaki Kobayashi is acknowledged for his helpful discussion.

References

Acharya and Beaudoin, 2000, Grain-size effect in viscoplastic polycrystals at moderate strains, J. Mech. Phys. Sol., 48, 2213-2230

Acharya, Bassani and Beaudoin, 2003, Geometrically necessary dislocations, hardening, and a simple gradient theory of crystal plasticity, Scripta Mat., 48, 167-172

Akasheh, F., Zbib, H.M., and Ohashi, T., 2006, Multiscale modeling of size effect in FCC crystals: discrete dislocation dynamics and density based gradient crystal plasticity, to be published in Phil. Mag.

Benzerga, A. A. and Shaver, N. F., 2006, Scale dependence of mechanical properties of single crystals under uniform deformation, Scripta Mat., 54, 1937-1941.

Benzerga, A.A., Bréchet, Y., Needleman, A. and Van der Giessen, E., 2004, Incorporating three-dimensional mechanisms into two-dimensional dislocation dynamics, Modelling Simul. Mater. Sci. Eng., 12, 159-196.

Berbenni, S., Favier, V. and Berveiller, M., 2006, Impact of the grain size distribution on the yield stress of heterogeneous materials, Int. J. Plasticity, (article in press).

Cheong, K.S., Busso, E.P. and Arsenlis, A., 2005, A study of microstructural length scale effects on the behaviour of FCC polycrystals using strain gradient concepts, Int. J. Plasticity, 21, 1797-1814.

Chronological Science Tables, 2001, National astronomical observatory ed., Maruzen Co., pub., Tokyo, 453.

Fleck, N.A., Muller, G.M., Ashby, M.F. and Hutchinson, J.W., Strain gradient plasticity: Theory and experiment, 1994, Acta metall. mater., 42, 475.

Fredriksson, P. and Gudmundson, P., 2005, Size-dependent yield strength of thin films, Int. J. Plasticity, 21, 1834-1854.

Gao, H., Huang, Y., Nix, W.D., and Hutchinson, J.W., 1999, Mechanism-based strain gradient plasticity— I. Theory, J. Mech Phys Solids. 47, 1239.

Gurtin, M.E., 2002, A gradient theory of single-crystal viscoplasticity that accounts for geometrically necessary dislocations, J. Mech. Phys. Solids, 50, 5-32.

Hull, D. and Bacon, D.J., 2001, Introduction to dislocations, 4th Ed. Butterworth Heinemann, 150.

Hirth, J.P. and Lothe, J., 1982, Theory of dislocations, John Wiley & Sons., New York, 132.

Hirth, J.P., Zbib, H.M. and Lothe J., 1998, Forces on high velocity dislocations, Modeling & Simulations in Maters. Sci. & Eng, 6, 165-169.

Khan, A.S., Suh, Y.S., Chen, X., Takacs, L. and Zhang, H., 2006, Nanocrystalline aluminum and iron: Mechanical behavior at quasi-static and high strain rates, and constitutive modeling, Int. J. Plasticity, 195-209.

Mesarovic, S.Dj, 2005, Energy, configurational forces and characteristic lengths associated with

the continuum description of geometrically necessary dislocations, Int. J. Plasticity, 21, 1855-1889.

Ohashi, T., 1994, Numerical modeling of plastic multi slip in metal crystals of face centered cubic type, Phil. Mag. A70, 793-803.

Ohashi, T., 1997, Finite element analysis of the plastic slip and evolution of the geometrically necessary dislocations in F.C.C. crystals, Phil. Mag. Lett., 75, 51-57.

Ohashi, T., 2004a, A new model of scale dependent crystal plasticity analysis, Solid mech. appl., vol. 115, Proc. IUTAM symposium on mesoscopic dynamics in fracture process and strength of materials, Kluwer Academic Pub., Dordrecht, eds., H. Kitagawa and Y. Shibutani, 97-106.

Ohashi, T., 2004b, Three dimensional structures of the geometrically necessary dislocations in matrix-inclusion systems under uniaxial tensile loading, Int. J. Plast., 20, 1093-1109.

Ohashi, T. and Kawamukai, M., 2005, Scale dependency in yield stress of polycrystalline metals, Proc. 18th JSME Comp. Mech. Conf., Tsukuba, Japan, pp. 87-88 (in Japanese).

Ohashi, T., 2005, Crystal plasticity analysis of dislocation emission from micro voids, Int. J. Plast., 21, 2071-2088.

Press, W.H., et al, 1996, Numerical recipes in Fortran77, second ed. Cambridge press, Cambridge, 346.

Shizawa, K. and Zbib, H.M., 1999, A thermodynamical theory of gradient elastoplasticity with dislocation density tensor. I: Fundamentals, Int. J. Plast., 15, 899-938.

Shu, J.Y. and Fleck, N.A., 1999, Strain gradient crystal plasticity: size-dependent deformation of bicrystals, J. Mech. Phys. Solids, 47, 297

Simmons, G. and Wang, H., 1997, Single crystal elastic constants and calculated aggregate properties: A handbook, second ed., MIT press, Cambridge, 23.

Uchic, M.D., Dimiduk, D.M., Florando, J.N. and Nix, W.D., 2004, Sample dimension s influence strength and crystal plasticity, Science, vol. 305, 986-989.

Zbib, H.M., and Khraishi, T.A., 2005, Dislocation Dynamics, in: Handbook of materials modeling, ed. Sidney Yip, pp1097-1114, Springer.

Zbib, H.M., and Diaz de la Rubia, T., A multiscale model of plasticity, 2002, Int. J. Plast., 18, 1133-1163.

Figure captions

Fig.1 (a) Cuboidal-shaped crystal grain employed for the dislocation dynamics simulation. A dislocation segment aa' lies on the slip plane and operates as a Frank-Read source. (b) Geometry of the slip plane, Frank-Read source and Burgers vector.

Fig.2 Formation of a closed dislocation loop in a crystal grain surrounded by rigid walls when $d = 1$ and $\lambda = 0.2$ μm. At this condition, $\tau_\infty = 60.375\,MPa$. The applied shear stress is $\tau = 62\,MPa = 1.027\tau_\infty$.

Fig.3 Expansion of a dislocation arc when $d/\lambda = 2$ and $\tau = 1.9\tau_\infty$. $d = 1$ and $\lambda = 0.5$ μm.

Fig.4 Growth of dislocation loops that were generated from F-R sources at two positions near grain boundaries. $d/\lambda = 5$. $d = 1$ and $\lambda = 0.2$ μm. $\tau_\infty = 60.375$, $\tau_{applied} = 62\,MPa$

Fig.5 Emission of dislocation loops from two F-R sources.

Fig.6 Relation between τ_{thres}/τ_∞ and d/λ. Data depicted by filled symbols were obtained by simulation limited to 750,000 steps, while the datum given by open symbol △ for $\lambda = 10\,\mu m$ was obtained by simulation limited to 7,500,000 steps.

Fig.7 Plot of $\log(\beta)$ against $\log(\lambda)$. Data were obtained by simulation limited to 750,000 steps.

Fig.8 (a) Polycrystal model employed for the finite element crystal plasticity analysis. The model consists of six grains, and aspect ratio of the specimen is W:H:D=5:15:1. Mean grain diameter $\bar{d}$ is assumed to be equal to W. (b) Crystal orientation for each grain.

Fig.9 Nominal stress – nominal strain curves when grain boundary effect is not taken into account (β=0). (a) Details at yielding, (b) strain hardening behavior after yielding, obtained in Ohashi, 2004a where some material data are different from those used in Fig. 9(a), Fig. (10) and (11); a=0.1, c*=100 θ_0=0 are used.

Fig.10 Nominal stress versus nominal strain curves obtained for three specimens with $\bar{d}$ =1, 5 and 50 μm. The total initial dislocation density is $\rho_0^{total} = 1.2 \times 10^{12}, m^{-2}$, and it is assumed that $\beta = 1$. The first plastic slip takes place at points A, B, and C in the specimens with $\bar{d}$ =1, 5 and 50 μm, respectively. Macroscopic yield points are indicated by points A', B' and C'.

Fig.11 Nominal stress versus nominal strain curves obtained for three specimens with $\bar{d}$ =1, 5 and 50 μm when the total initial dislocation densities are (a) $\rho_0^{total} = 1.2 \times 10^{13}, m^{-2}$ and (b) $\rho_0^{total} = 1.2 \times 10^{14}, m^{-2}$. It is assumed that $\beta = 1$. Variation of the macroscopic yield points, as well as the points of onset of microscopic plastic slip, is less prominent when the initial dislocation density is larger.

Fig.12 Macro- and microscopic yield stresses plotted against mean grain diameter $\bar{d}$. Filled symbols show macroscopic yield stress and open symbols indicate microscopic yield stress at which plastic slip deformation first take place in the specimen. The gradient is not a constant but varies with mean grain diameter and initial dislocation density.

Table 1 Material constants used for dislocation dynamics simulation.

Density of mass, kg/m^3	8960
Elastic constants	
Shear modulus μ [(1)], Pa	4.83×10^{10}
Poisson's ratio[(1)]	0.343
Dislocation mobility constant, 1/Pa·s	1000
Magnitude of Burger's vector $\tilde{b}$, m	2.5×10^{-10}
Lattice friction stress	$10^{-5} \times \mu = 0.483$ MPa
Temperature, K	300

[(1)] Experimental data obtained for copper polycrystals (Chronological Science Tables, 2001).

Table 2 Time needed for the emission of a dislocation loop t_{emit} and the dislocation dynamics simulation steps.

λ, m	$\tau_{thres} / \tau_{\infty}$	d / λ	t_{emit}, s	DD step, 10^3	max. DD step, 10^3
1.00E-06	1.184	10	1.50E-05	43	3,000
2.00E-06	0.994	10	2.05E-04	54	↑
5.00E-06	1.077	10	1.74E-04	95	↑
1.00E-05	1.49	10	3.73E-03	1002	7,500
1.00E-05	4.33	1.8	9.58E-05	255	750
1.00E-05	3.50	2	1.81E-04	481	↑
1.00E-05	2.67	2.5	1.87E-04	497	↑
1.00E-05	2.17	3	2.26E-04	600	↑
1.00E-05	2.00	5	2.82E-04	747	↑
1.00E-05	2.00	10	2.51E-04	656	↑
5.00E-07	2.774	1.8	3.30E-07	10	↑
5.00E-07	2.319	2	9.01E-07	25	↑
5.00E-07	1.449	2.8	1.18E-06	23	↑
5.00E-07	1.325	3	1.68E-06	30	↑
5.00E-07	1.201	3.6	3.41E-05	538	↑
5.00E-07	1.201	4	2.29E-05	306	↑
5.00E-07	1.201	8	1.43E-06	10	↑
3.00E-07	1.267	3	4.65E-07	14	↑
3.00E-07	1.168	3.333	6.57E-07	18	↑
3.00E-07	1.118	4.667	2.65E-06	51	↑
3.00E-07	1.093	5	5.21E-07	10	↑
3.00E-07	1.068	6	5.58E-07	9	↑
3.00E-07	1.068	6.667	5.45E-07	8	↑

Table 3 Material constants used for crystal plasticity analysis.

Elastic compliances[(1)], 10^{-11} Pa^{-1}	s_{11}=1.4943, s_{12}=-0.6257, s_{44}=1.3214
Shear modulus μ in eq. (12b), Pa	$1/s_{44}= 7.57 \times 10^{10}$
a in Eq. (12b)	0.3
β in Eq. (12b)	1
c in Eq. (7)	1
c* in Eq. (8)	15
Lattice friction stress θ_0 in Eq. (12b), MPa	0.483

[(1)] Simmons and Wang, 1971.

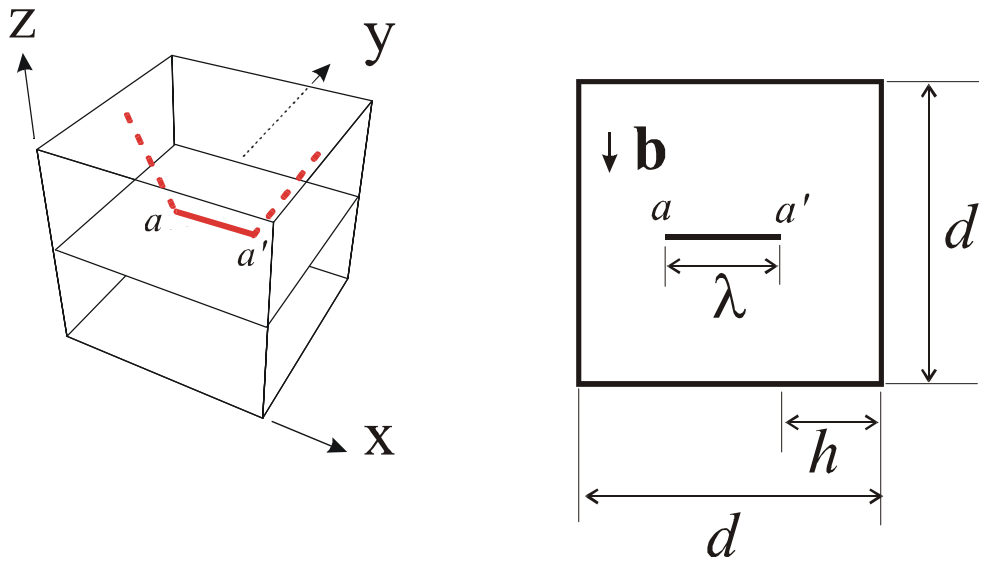

(a) (b)

Fig.1 (a) Cuboidal-shaped crystal grain employed for the dislocation dynamics simulation. A dislocation segment aa' lies on the slip plane and operates as a Frank-Read source. (b) Geometry of the slip plane, Frank-Read source and Burgers vector.

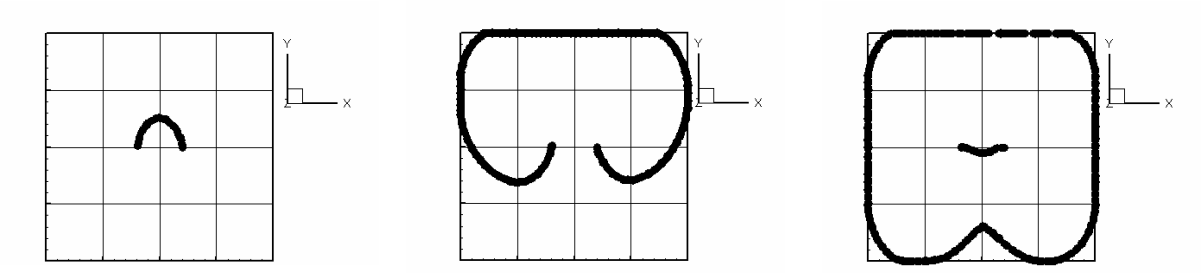

(a) (b) (c)

Fig.2 Formation of a closed dislocation loop in a crystal grain surrounded by rigid walls when $d = 1$ and $\lambda = 0.2$ μm. At this condition, $\tau_\infty = 60.375\,MPa$. The applied shear stress is $\tau = 62\,MPa = 1.027\tau_\infty$

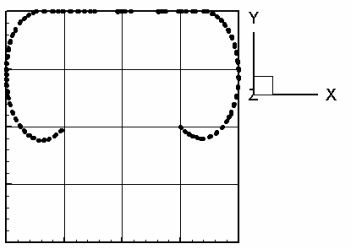

Fig.3 Expansion of a dislocation arc when $d/\lambda = 2$ and $\tau = 1.9\tau_\infty$. $d = 1$ and $\lambda = 0.5$ μm.

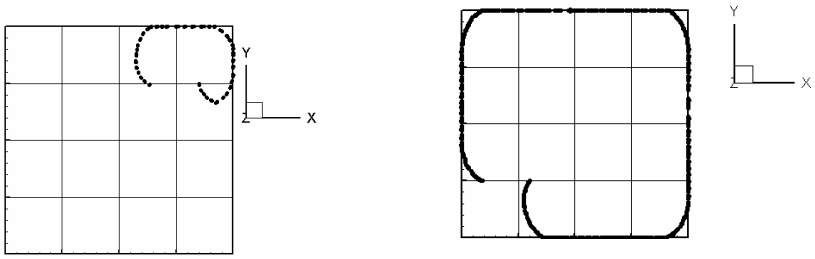

(a) (b)

Fig.4 Growth of dislocation loops that were generated from F-R sources at two positions near grain boundaries. $d/\lambda = 5$. $d = 1$ and $\lambda = 0.2$ μm. $\tau_{\infty} = 60.375, \tau_{applied} = 62\,MPa$

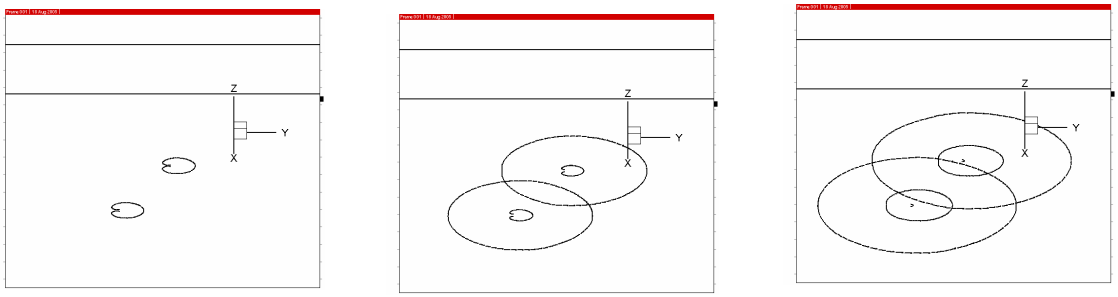

(a) (b) (c)

Fig.5 Emission of dislocation loops from two F-R sources.

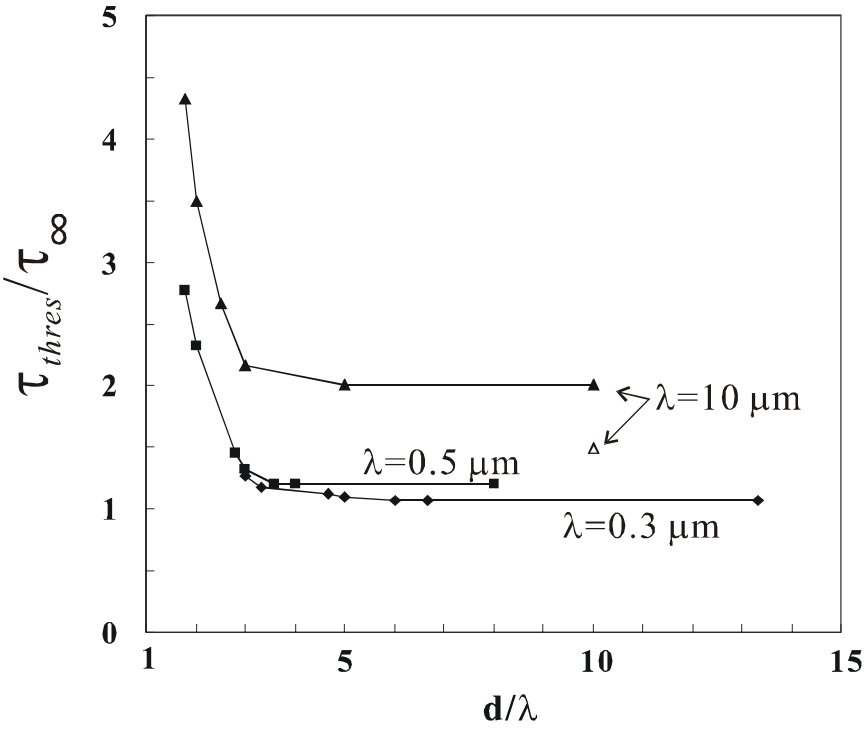

Fig.6 Relation between $\tau_{thres}/\tau_{\infty}$ and d/λ. Data depicted by filled symbols were obtained by simulation limited to 750,000 steps, while the datum given by open symbol ▵ for $\lambda = 10\,\mu m$ was obtained by simulation limited to 7,500,000 steps.

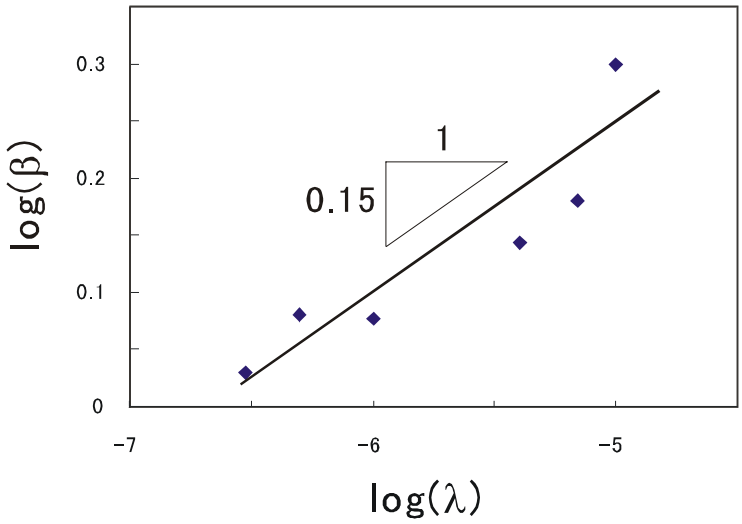

Fig.7 Plot of $\log(\beta)$ against $\log(\lambda)$. Data were obtained by simulation limited to 750,000 steps .

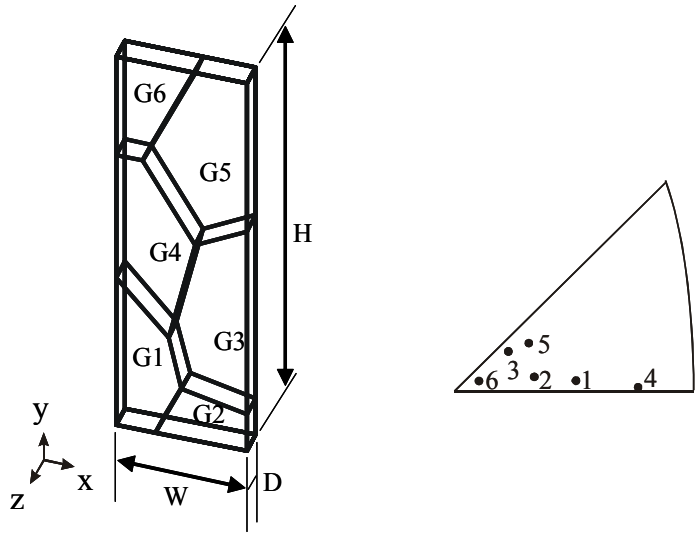

Fig.8 (a) Polycrystal model employed for the finite element crystal plasticity analysis. The model consists of six grains, and aspect ratio of the specimen is W:H:D=5:15:1. Mean grain diameter $\bar{d}$ is assumed to be equal to W. (b) Crystal orientation for each grains.

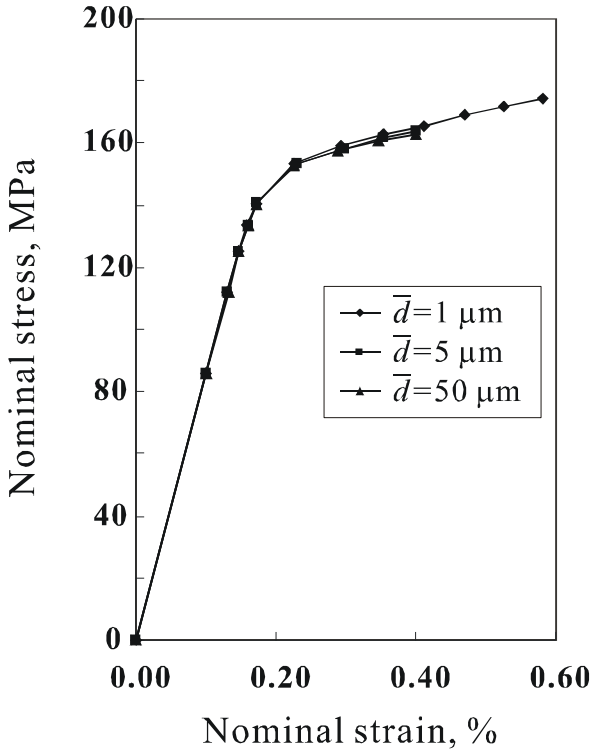

(a)

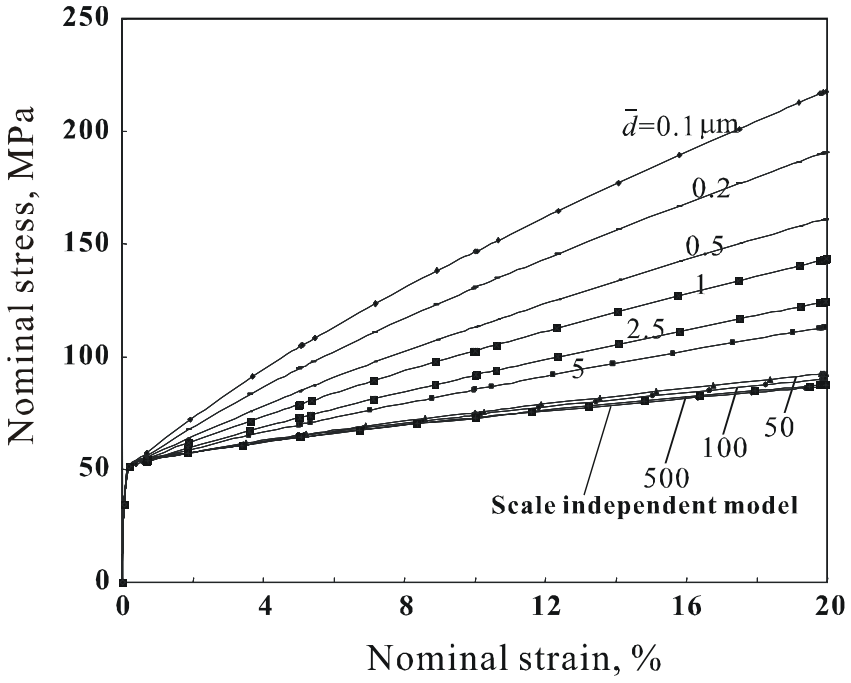

(b)

Fig.9 Nominal stress – nominal strain curves when grain boundary effect is not teken into account (β=0). (a) Details at yielding, (b) strain hardening behavior after yielding, obtained in Ohashi, 2004a where some material data are different from those used in Figs. 9(a), (10) and (11); a=0.1, c*=100 θ_0=0 are used.

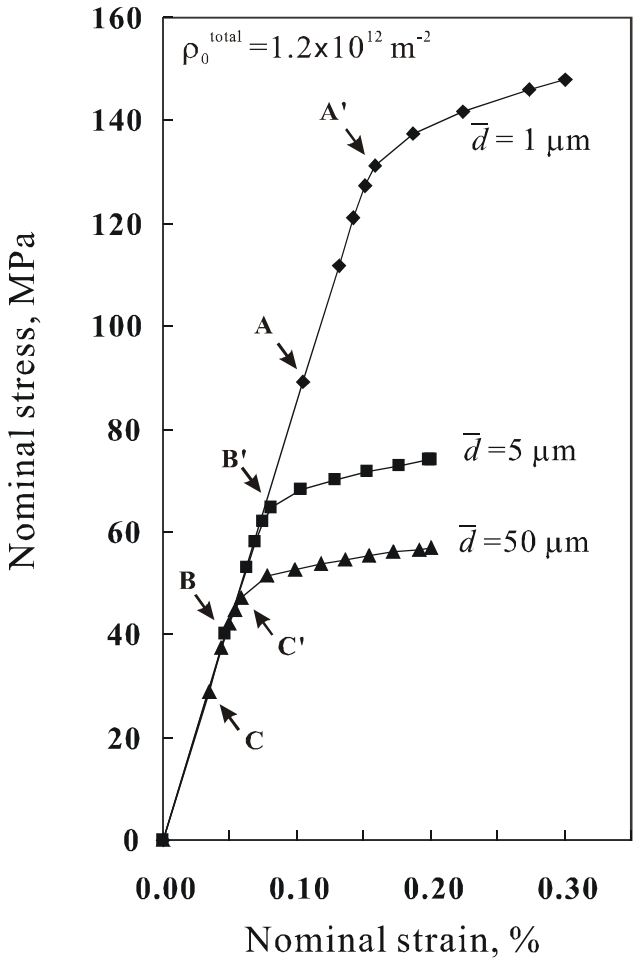

Fig.10 Nominal stress versus nominal strain curves obtained for three specimens with $\bar{d}$ =1, 5 and 50 μm. The total initial dislocation density is $\rho_0^{total} = 1.2 \times 10^{12}, m^{-2}$, and it is assumed that $\beta = 1$. The first plastic slip takes place at points A, B, and C in the specimens with $\bar{d}$ =1, 5 and 50 μm, respectively. Macroscopic yield points are indicated by points A', B' and C'.

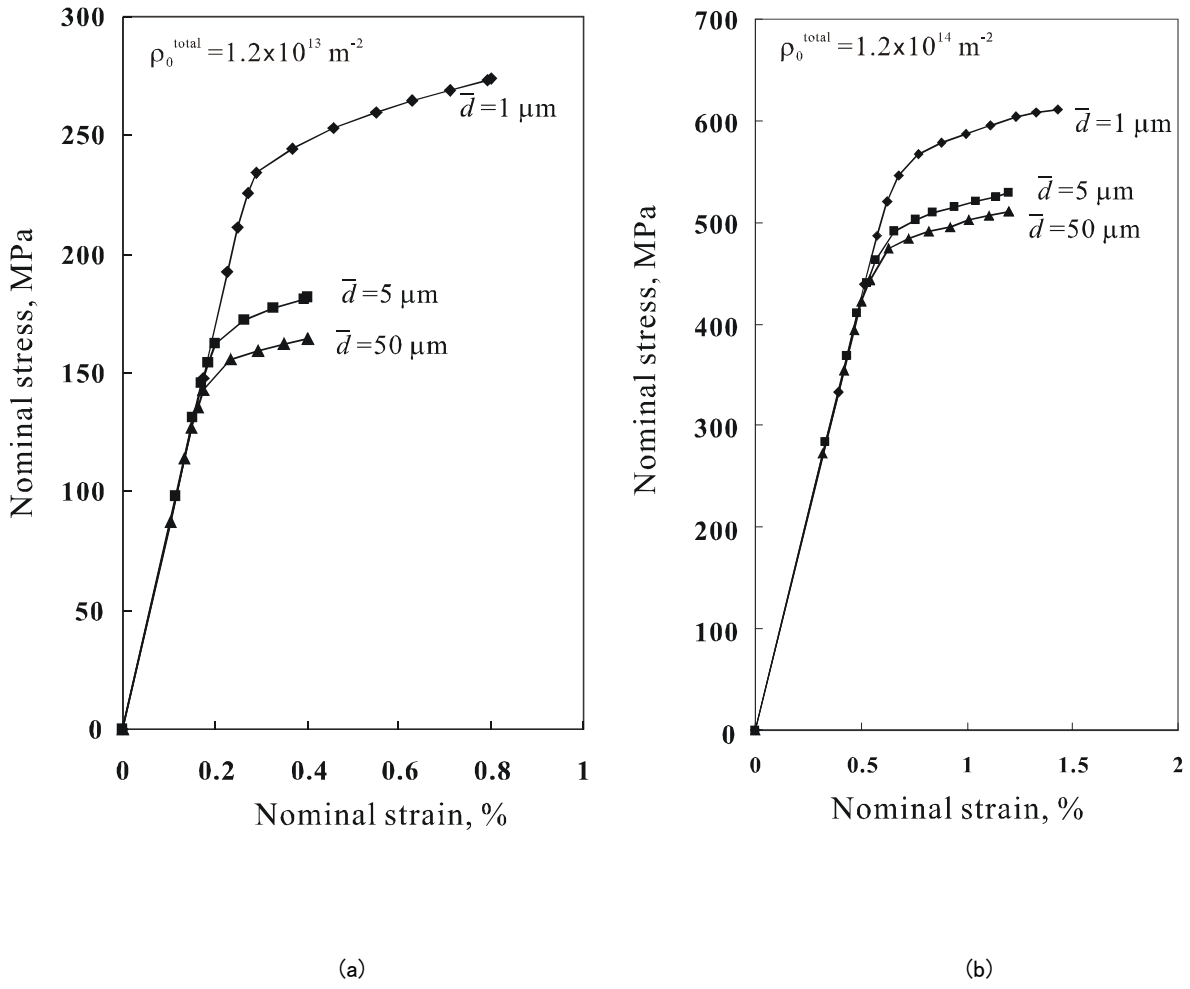

Fig.11 Nominal stress versus nominal strain curves obtained for three specimens with $\overline{d}$ =1, 5 and 50 μm when the total initial dislocation densities are (a) $\rho_0^{total} = 1.2 \times 10^{13}, m^{-2}$ and (b) $\rho_0^{total} = 1.2 \times 10^{14}, m^{-2}$. It is assumed that $\beta = 1$. Variation of the macroscopic yield points, as well as the points of onset of microscopic plastic slip, is less prominent when the initial dislocation density is larger.

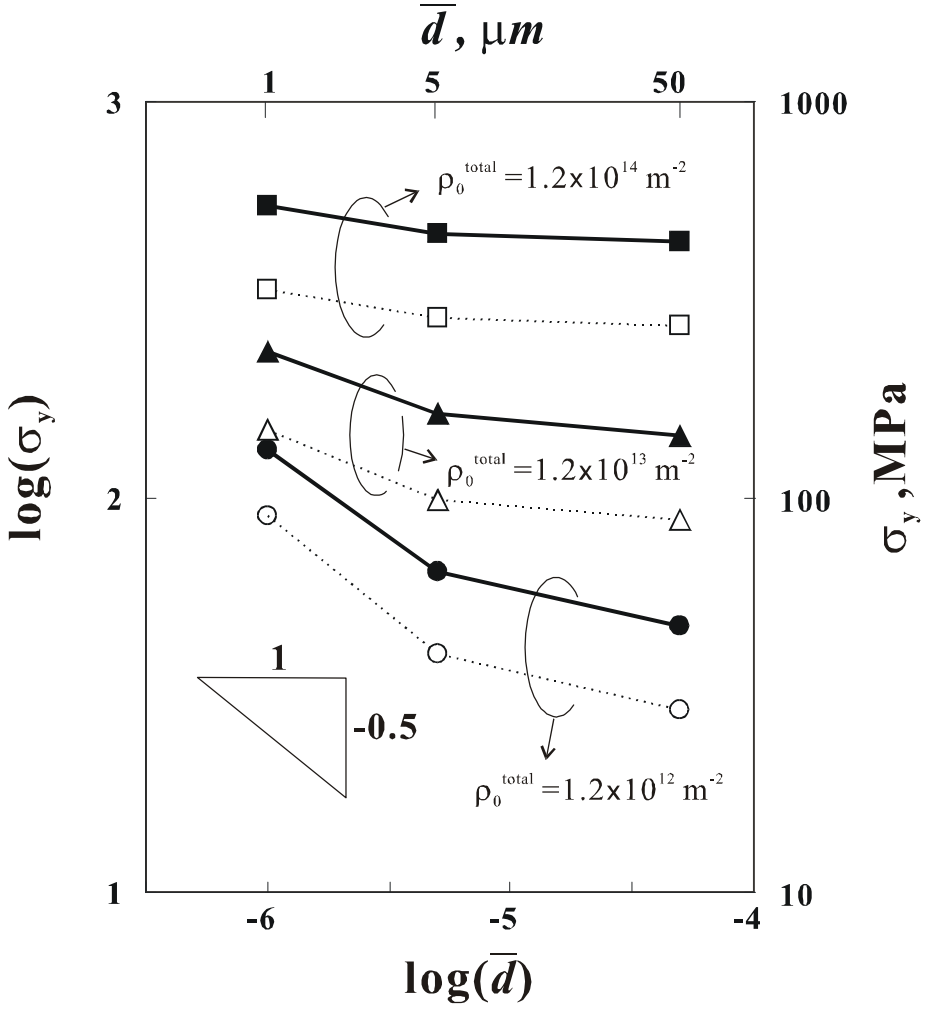

Fig.12 Macro- and microscopic yield stresses plotted against mean grain diameter $\overline{d}$. Filled symbols show macroscopic yield stress and open symbols indicate microscopic yield stress at which plastic slip deformation first take place in the specimen. The gradient is not a constant but varies with mean grain diameter and initial dislocation density.